Possibilities and Limits of Avalanche Lasing on the Green Er^{3+}:LiYF$_4$ Transition

M. Pollnau, W. Lüthy, and H. P. Weber

Institute of Applied Physics, University of Bern, Sidlerstr. 5, CH-3012 Bern, Switzerland

Abstract

In computer simulations the population mechanisms of the room-temperature continuous-wave green up-conversion Er^{3+}:LiYF$_4$ laser are investigated. An avalanche process is the dominating excitation mechanism, but it also counteracts stimulated emission at higher dopant concentrations. This concentration dependence can be considered as a behaviour present in many rare-earth-doped avalanche lasers.

Introduction

One of the interests in solid-state laser physics has focused on diode-pumped upconversion lasers for possible applications in the field of data storage. Stimulated emission on the green erbium transition $^4S_{3/2} \rightarrow {}^4I_{15/2}$ at cryogenic temperatures has first been reported in 1972 [1]. In diode-pumped upconversion-lasing experiments considerably high output powers have been achieved [2]. The first report on room-temperature lasing in Er^{3+}:LiYF$_4$ at 551 nm [3] has evoked further efforts in the investigation of this laser. Recently upconversion-pumped cw-laser operation has been demonstrated [4,5] with a laser threshold in the range of 1 W. However, the understanding of the processes that lead to cw lasing is far from being complete.

In this contribution the complicated population mechanisms of the Er^{3+}:LiYF$_4$ laser system are analyzed in a computer simulation. The rate-equation scheme considers all excited levels up to $^2H_{9/2}$, ground-state depletion, excited-state absorption (ESA) on the pump and laser wavelength, three upconversion processes as well as their inverse processes, stimulated emission, and the crystal and resonator data of the experiments. An avalanche process appears to be the dominant excitation mechanism of the upper laser level, but the same process also limits the possible range of dopant concentration due to the quenching of the lifetime of the upper laser level. This limitation seems to be a general aspect of many avalanche lasers.

Computer Simulation

The labelling of the levels considers the energetic order of the Er^{3+} level system (see Fig. 1). Since the $^2H_{11/2}$ and $^4S_{3/2}$ levels as well as the $^4F_{5/2}$ and $^4F_{3/2}$ levels are thermally coupled with each other they are treated as combined levels with a Boltzmann-population distribution. The Er^{3+}:LiYF$_4$ parameter set used in our rate-equation model is taken from Refs. [3-7]. The intrinsic lifetimes of the levels (see Fig. 1) include radiative transitions and multiphonon relaxation. The radiative transition rates are known from a Judd-Ofelt calculation [6]. The nonradiative transition rates and the branching ratios β_{ij} are calculated as shown in Ref. [8].

Three ion-ion interactions W$_{ij}$ are taken into account (see Fig. 1). The parameters W_{11} and W_{22} of the sample doped with 1 % Er^{3+} are assumed to have half the values measured [7] for the 10 % sample. The parameter W_{50} is derived from our computer simulation. The inverse processes (not shown in Fig. 1) are also considered. Since for the processes W$_{22}$ and W$_{50}$ there is a full spectral overlap between the involved manifold transitions the normal and inverse parameters are assumed to have the same values. For W$_{11}$ there is only a phonon-assisted overlap.

The processes $^4I_{13/2} \rightarrow {}^4I_{15/2}$ and $^4I_{13/2} \rightarrow {}^4I_{9/2}$ have stronger transitions in the relevant area than the inverse processes due to different Boltzmann populations of the same transition in absorption and emission. A brief evaluation of normal and inverse parameter considers the assistance of one phonon with energy $h\nu_{ph} = 400$ cm^{-1} and includes all Stark transitions in the phonon-assisted overlap region with the same atomic cross section and the Boltzmann populations of the initial levels at 300 K. Summing all contributions for the normal and the inverse process results in $W_{11} = 2.5 \times W_{30}$, which is tentatively used for the determination of W_{30}. With the assumption $W_{11} = W_{30}$ the experimental results could not be reproduced.

The following set of parameters [4,5] is used in the simulation: crystal length $\ell = 4$ mm, dopant concentration $N_0 = 1.37 \times 10^{20}$ cm^{-3}, a concentric resonator of optical length $\ell_{opt} = 0.1$ m, losses due to scattering and diffraction $L_r = 0.05$. The erbium
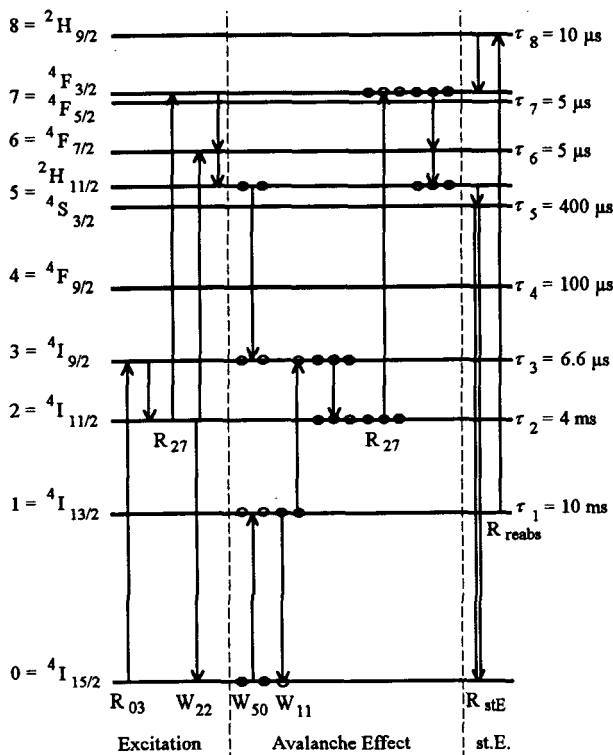

Figure 1. Energy level scheme of Er^{3+}(1%):LiYF$_4$ indicating the processes which are relevant for the population and deexcitation of the $^4S_{3/2}$ upper laser level at the pump wavelength $\lambda_p = 810$ nm. (a) Excitation of the upper laser level, (b) the avalanche effect, and (c) stimulated emission and ESA on the laser wavelength.

ions are pumped with a Ti:sapphire laser at wavelength $\lambda_p = 810$ nm by GSA $^4I_{15/2} \rightarrow {}^4I_{9/2}$ (cross section $\sigma_{03} = 8.5 \times 10^{-22}$ cm^2) and ESA $^4I_{11/2} \rightarrow {}^4F_{3/2}$ ($\sigma_{27} = 5 \times 10^{-21}$ cm^2). No significant ESA from the $^4I_{13/2}$ level occurs at 810 nm [9]. The transmission of the incoupling optics is $\eta_T = 0.9$, the average radius of the laser beam within the crystal $r_{mode} = 20$ μm, the overlap between pump and laser mode $\eta_B = 0.9$.

The laser transition starts from the second Stark level of $^4S_{3/2}$ (Boltzmann population $b_{52} = 0.402$ at 300 K, degeneracy $g_{52} = 2$) and terminates in the eighth Stark level of $^4I_{15/2}$ ($b_{08} = 0.042$, $g_{08} = 2$) at $\lambda_{Laser} = 551.3$ nm ($\sigma_{50} = 5 \times 10^{-20}$ cm^2). Only the fraction $P_1 / P = 10^{-7}$ of the spontaneous emission is emitted into the laser mode. Reabsorption losses R_{reabs} due to ESA [10] from $^4I_{13/2}$ ($b_{11} = 0.220$, $g_{11} = 2$) into $^2H_{9/2}$ ($b_{84} = 0.142$, $g_{84} = 2$) are considered dynamically with $\sigma_{18} = 5 \times 10^{-22}$ cm^2. The transmission of the outcoupling mirror is $T = 3$ %.

The rate equations for the population densities N_i, the photon density ϕ, the stimulated-emission rate R_{stE}, and the reabsorption rate R_{reabs} are given by

$$dN_8/dt = R_{reabs} - \tau_8^{-1}N_8 \tag{1}$$

$$dN_7/dt = R_{27}N_2 - \tau_7^{-1}N_7 + \beta_{87}\tau_8^{-1}N_8 \tag{2}$$

$$dN_6/dt = -\tau_6^{-1}N_6 + \Sigma_{i=7..8}(\beta_{i6}\tau_i^{-1}N_i)$$
$$+ W_{22}N_2{}^2 - W_{60}N_6N_0 \tag{3}$$

$$dN_5/dt = -\tau_5^{-1}N_5 + \Sigma_{i=6..8}(\beta_{i5}\tau_i^{-1}N_i)$$
$$- W_{50}N_5N_0 + W_{13}N_1N_3 - R_{stE} \tag{4}$$

$$dN_4/dt = -\tau_4^{-1}N_4 + \Sigma_{i=5..8}(\beta_{i4}\tau_i^{-1}N_i) \tag{5}$$

$$dN_3/dt = R_{03}N_0 - \tau_3^{-1}N_3 + \Sigma_{i=4..8}(\beta_{i3}\tau_i^{-1}N_i)$$
$$+ W_{50}N_5N_0 - W_{13}N_1N_3$$
$$+ W_{11}N_1{}^2 - W_{30}N_3N_0 \tag{6}$$

$$dN_2/dt = -R_{27}N_2 - \tau_2^{-1}N_2 + \Sigma_{i=3..8}(\beta_{i2}\tau_i^{-1}N_i)$$
$$- 2W_{22}N_2{}^2 + 2W_{60}N_6N_0 \tag{7}$$

$$dN_1/dt = -\tau_1^{-1}N_1 + \Sigma_{i=2..8}(\beta_{i1}\tau_i^{-1}N_i)$$
$$+ W_{50}N_5N_0 - W_{13}N_1N_3$$

$$-2W_{11}N_1^2+2W_{30}N_3N_0-R_{reabs} \quad (8)$$

$$dN_0/dt = -R_{03}N_0+\Sigma_{i=1..8}(\beta_{i0}\tau_i^{-1}N_i)$$

$$-W_{50}N_5N_0+W_{13}N_1N_3$$

$$+W_{11}N_1^2-W_{30}N_0N_3$$

$$+W_{22}N_2^2-W_{60}N_0N_6+R_{stE} \quad (9)$$

$$d\phi/dt = (\ell/\ell_{opt})[(P_l/P)\beta_{50}\tau_5^{-1}N_5+R_{stE}-R_{reabs}]$$

$$+\ln[(1-T)(1-L_r)]c\phi/2\ell_{opt} \quad (10)$$

$$R_{stE} = [b_{52}N_5-(g_{52}/g_{08})b_{08}N_0]\sigma_{50}c\phi \quad (11)$$

$$R_{reabs} = [b_{11}N_1-(g_{11}/g_{84})b_{84}N_8]\sigma_{18}c\phi \quad (12)$$

The equation for the pump rates including ESA and bleaching of the ground state is

$$R_{ij} = [\sigma_{ij}/(\sigma_{03}N_0+\sigma_{27}N_2)]\cdot[\lambda_p/(hc\ell\pi r_{mode}^2)]\cdot$$

$$[1-\exp\{-(\sigma_{03}N_0+\sigma_{27}N_2)\ell\}]\eta_T\eta_BP_{in}. \quad (13)$$

The rate-equation system is solved in a Runge-Kutta calculation of fourth order. The investigation of the population mechanisms leads to results explained in the following paragraphs.

Pump Excitation of the Upper Laser Level

At the pump wavelength 810 nm the GSA $^4I_{15/2} \rightarrow$ $^4I_{9/2}$ populates the $^4I_{11/2}$ level via multiphonon relaxation. The ESA from the $^4I_{11/2}$ level and the upconversion W_{22} populate the upper laser level $^4S_{3/2}$, see the left part of Fig. 1. The best overlap between GSA and ESA cross sections leads to the highest laser output at 551 nm, in agreement with experiments [4,5].

A stronger upconversion W_{22} is decreasing the laser output due to the following reason. Owing to the low dopant concentration and the small GSA cross section only a small part of the pump power is absorbed in the crystal. An increase of the population of either the GSA or the ESA pump level linearly increases the absorbed pump power on the corresponding transition. The upconversion W_{22} removes two excitations from the ESA pump level, but transfers only one of them into the upper laser level. Without upconversion both excitations could be pumped via ESA into the upper laser level.

The Avalanche Effect

Since the GSA is weak the two-step excitation of the upper laser level via GSA and ESA would only lead to a small inversion on the laser transition. Therefore, other excitation mechanisms gain importance. The computer simulation gives evidence that an avalanche process strongly supports the excitation of the crystal, see the central part of Fig. 1. The cross relaxation W_{50} from the upper laser level repopulates the ESA pump level. In addition it excites the $^4I_{13/2}$ level from the ground state. Half of this additional excitation is transferred into the ESA pump level by an upconversion. Although the parameter W_{11} for this upconversion has a small value at 1 % Er^{3+} concentration, the long $^4I_{13/2}$ lifetime and its high population due to the cross relaxation lead to a strong upconversion rate.

One avalanche cycle starts with two excitations in the upper laser level and finishes with three excitations in the upper laser level (see Fig. 1), which is an enhancement factor of 1.5. At moderate pump powers this excitation channel is more efficient than the weak GSA. An intensity threshold observed in other systems [11,12,13,14] for the onset of the avalanche effect cannot be observed in this case because GSA is present.
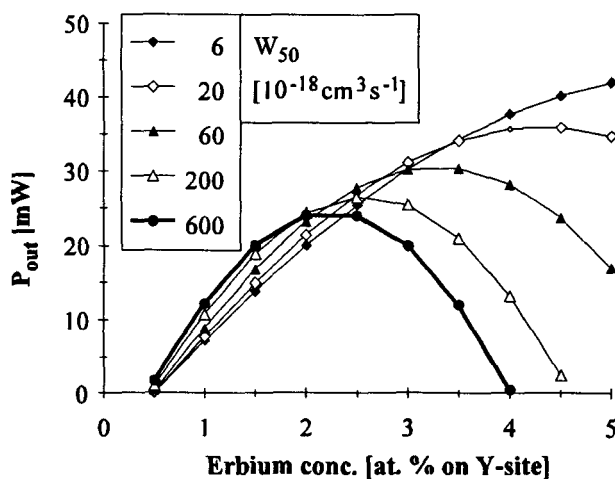

Figure 2. The dependence of output power on dopant concentration for different parameters of the cross relaxation W_{50} from the $^4S_{3/2}$ upper laser level. At 1 % dopant concentration a stronger cross relaxation increases the laser output which demonstrates the avalanche effect. The value $600 \times 10^{-18} cm^3 s^{-1}$ corresponds to the experimentally observed quenching of the output power with rising dopant concentration.

The Concentration Dependence

The cross relaxation W_{50} leads to efficient avalanche lasing at low dopant concentrations. On the other hand this cross relaxation depletes the upper laser level [15]. The effect of the cross relaxation W_{50} at different dopant concentrations is shown in Fig. 2: At 1 % conc. a stronger cross relaxation increases the laser output, which demonstrates the avalanche effect. At considerably higher dopant concentrations the rate of W_{50} successfully competes with stimulated emission. This decreases the output power and limits the possible range of dopant concentration. The parameter which reproduces the experimental results for the laser output at 1 % conc. and gives a good explanation of the experimentally observed concentration dependence is $W_{50} = W_{13} = 6$ (±4) x 10^{-22} m^{3}s^{-1} (thick line in Fig. 2).

Owing to the quenching effect of the cross relaxation a considerably higher erbium concentration cannot be used for the enhancement of the GSA and ESA. This would otherwise be useful for a better pump absorption and would increase the laser output.
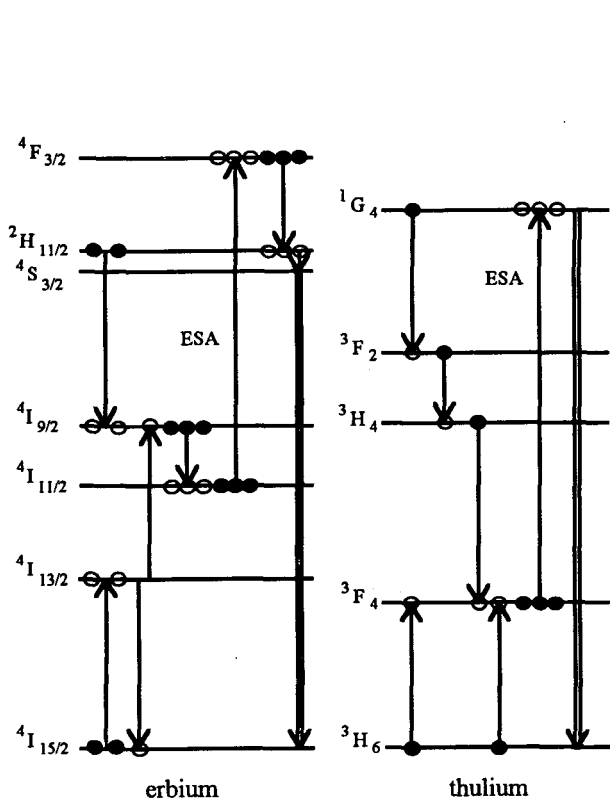
General Aspects of Avalanche Excitation

The photon-avalanche effect has been observed in several rare-earth-doped solid-state materials, e.g. in Pr^{3+}:LaCl$_3$ [11], Tm^{3+}:YAG [12,13], and Nd^{3+}:LiYF$_4$ [14]. The different enhancement factors of 1.5 for Er^{3+}:LiYF$_4$, 2 for Pr^{3+}:LaCl$_3$ and Nd^{3+}:LiYF$_4$, and 3 for Tm^{3+}:YAG are compared in the excitation schemes of Figs. 3 and 4.

The strong cross relaxation required for the avalanche effect must start from a highly populated (metastable) level. In rare-earth ions there can be found only a few metastable levels in the visible energy range above the ground state. Therefore, a coincidence of the initial levels of cross relaxation and stimulated emission and the quenching of the lifetime of the upper laser level at higher dopant concentrations is very likely to occur. In three examples of Figs. 3 and 4 the coincidence is present. In erbium the cross relaxation level is thermally connected to the upper laser level. The concentration dependence which has been observed in the case of Er^{3+} and Nd^{3+} can be considered as a general behaviour of many avalanche lasers.
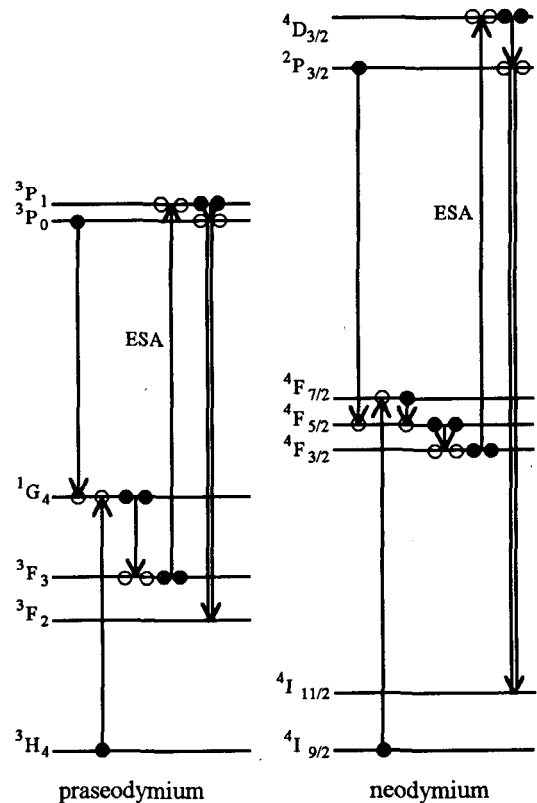

Figure 3. Avalanche effect with enhancement factors of 1.5 in Er^{3+}:LiYF$_4$ (left hand side) and 3 in Tm^{3+}:YAG (right hand side).

Figure 4. Avalanche effect with an enhancement factor of 2 in Pr^{3+}:LaCl$_3$ (left hand side) and Nd^{3+}:LiYF$_4$ (right hand side).

Conclusions

We have analyzed the population mechanisms of the room-temperature cw Er^{3+}:$LiYF_4$ laser at 551 nm. An avalanche effect which exploits the strong cross relaxation from the upper laser level and the upconversion from $^4I_{13/2}$ is mainly responsible for the population of the ESA pump level. At higher dopant concentrations the cross relaxation becomes detrimental to stimulated emission due to the depletion of the upper laser level. This concentration dependence can be considered as a general feature of many rare-earth-doped avalanche lasers.

Acknowledgments

References

[1] L. F. Johnson and H. J. Guggenheim, Appl. Phys. Lett. 20, 474 (1972).

[2] R. R. Stephens and R. A. McFarlane, Opt. Lett. 18, 34 (1993).

[3] R. Brede, T. Danger, E. Heumann, G. Huber, and B. H. T. Chai, Appl. Phys. Lett. 63, 729 (1993).

[4] F. Heine, E. Heumann, T. Danger, T. Schweizer, J. Koetke, G. Huber, and B. Chai, OSA Proceedings on Advanced Solid-State Lasers, Tso Yee Fan and Bruce H. T. Chai, eds. (Optical Society of America, Washington, DC 1994), Vol. 20, pp. 344-347.

[5] F. Heine, E. Heumann, T. Danger, T. Schweizer, J. Koetke, G. Huber, and B. Chai, in Conference on Lasers and Electro-Optics Europe Technical Digest, Amsterdam 1994, paper CMA6, pp. 3-4.

[6] C. Li, Y. Guyot, C. Linarès, R. Moncorgé, and M. F. Joubert, in Advanced Solid-State Lasers and Compact Blue-Green Lasers Technical Digest, 1993 (Optical Society of America, Washington, D.C., 1993), Vol. 2, p.423.

[7] H. Chou and H. P. Jenssen, in Tunable Solid State Lasers, Vol. 5 of the OSA Proceeding Series, M. L. Shand and H. P. Jenssen, eds. (Opt. Soc. Am., Washington, D.C., 1989), pp. 167-174.

[8] M. Pollnau, Th. Graf, J. E. Balmer, W. Lüthy, and H. P. Weber, Phys. Rev. A 49, 3990 (1994).

[9] M. Pollnau, E. Heumann, and G. Huber, Appl. Phys. A 54, 404 (1992).

[10] M. Pollnau, E. Heumann, and G. Huber, J. Lumin. 60+61, 842 (1994).

[11] M. E. Koch, A. W. Kueny, and W. E. Case, Appl. Phys. Lett. 56, 1083 (1990).

[12] D. P. Shepherd et. al., CLEO/Europe, Amsterdam 1994, postdeadline paper CPD1.8.

[13] S. Guy, M. F. Joubert, B. Jacquier, phys. stat. sol., to be published.

[14] W. Lenth and R. M. Macfarlane, J. Lumin. 45, 346 (1990).

[15] J. P. van der Ziel, F. W. Ostermayer Jr., and L. G. van Uitert, Phys. Rev. B 2, 4432 (1970).